Ref.TH.2112-CERN

GEOMETRICAL RELATION BETWEEN DIFFRACTIVE AND NON-DIFFRACTIVE TWO-BODY SCATTERING

J.P. Ader *) and R. Peschanski +)

CERN - Geneva

and

R. Lacaze ")

Département de Physique Théorique
Université de Genève

A B S T R A C T

We postulate a heuristic relation between crossing odd Regge contributions and the dominant diffractive component. The connection comes from a universality in impact parameter distributions of particle and antiparticle cross-sections. This relation, successfully compared with experiment, is used in order to investigate diffraction. A satisfactory description of the ISR derivative cross-section $\partial\sqrt{d\sigma}/\partial \ell n s$ is obtained from a dual peripheral model for the non-diffractive amplitudes. The underlying Pomeron exhibits characteristic features : large oscillations with an exponential fall-off in square root of momentum transfer and a universal length scale of the order of 0.5 Fermi.

A theoretical interpretation of our results from the t channel (accumulation of n Reggeon cuts) and the s channel (effective Regge cut in the impact parameter plane) points of view is suggested.

---

*) Address after January 1st, 1976 : Laboratoire de Physique Théorique, Université de Bordeaux I.

+) Address after February 1st, 1976 : Service de Physique Théorique, CEA, Saclay.

") On leave of absence from : Service de Physique Théorique, CEA, Saclay. With partial support from the Swiss National Fund.

Ref.TH.2112-CERN

13 January 1976

1. INTRODUCTION

The distinction between diffractive and non-diffractive scattering processes has existed for a long time. Diffraction, which is mainly invoked for elastic scattering, is analogous to the scattering of light by a dark disk and gives cross-sections which are more or less independent of energy. By contrast, non-diffractive processes decrease with energy as a power law and display different structures in momentum transfer distributions. Any attempt to explain two-body strong interactions is faced with this double aspect of scattering. For instance, the conventional Regge-pole approach seemed to give a unified description in terms of t-channel singularities, diffraction being connected with vacuum exchange and non-diffractive processes with other quantum numbers. But soon many features appeared to be different, such as the peak shrinkages, duality properties, etc. Many interesting attempts were made to understand these differences, in particular recent works using multi-Regge duality diagrams and their topological properties[1].

Here a rather different way is taken, based on geometrical properties of two-body scattering, i.e. properties of the interaction region in the impact parameter plane b. Recently numerous works have been devoted to this intuitively simple approach. Concerning diffraction let us quote among others, the eikonal model[2] and the geometrical scaling (GS) hypothesis[3], where typical geometrical concepts like form factors and interaction radius play the main role. In non-diffractive processes, impact parameter properties are particularly simple: the dual geometrical models[4,5] insist upon the peripherality of both dominant resonances and high-energy amplitudes. More generally, a kind of universality of the geometry seems to emerge from numerous amplitude analyses and models for inelastic reactions and their different helicity amplitude[6].

In this work we intend to show that antiparticle and particle-proton elastic scattering differ by their interaction radii, the impact parameter distributions remaining essentially identical in shape. This leads to a geometrical link between diffractive and non-diffractive processes.

Section 2 analyses the diffractive and non-diffractive contributions to elastic scattering from this simple description of s-u crossed channel ($p^{\pm}p$, $K^{\pm}p$, $\pi^{\pm}p$) elastic scattering (Section 2.1). Then the relation between the imaginary part of odd-signature amplitudes and the Pomeron derivative with respect to energy, is compared with data (Section 2.2). The even-signature amplitudes are then considered (Section 2.3), since a phenomenological definition of the Pomeron contribution at non-asymptotic energies is given. The resulting geometrical relation allows a fruitful enlargement of our knowledge of two-body scattering, since a description of non-diffractive processes can be transposed on diffractive contributions and vice versa.

In Section 3 our way to a geometrical Pomeron is traced. Noting that non-diffractive and diffractive observables linked by our relation must share the same functional dependence, the parametrization given by dual geometrical models[4,5] particularly the dual peripheral model[5], is chosen for the non-diffractive part. Then an amplitude form is deduced for the Pomeron, describing ISR data in terms of predicted geometrical characteristics except the typical scale which is divided by two (Section 3.2). The connection of this approach with various theoretical schemes, especially with a t-channel point of view, is given in Section 3.3.

Finally, some conclusions and a survey of results are given in Section 4. A special emphasis is put on possible further developments.

2. RELATING NON-DIFFRACTIVE SCATTERING TO DIFFRACTION

2.1 General considerations

Diffraction exhibits nice geometrical properties and seems mainly governed by the interaction radius[3]. However, in the spirit of any s-channel approach there is no reason to limit oneself to diffractive processes. Indeed, considering the unitarity condition for a given elastic process, it is difficult to assign the different multiparticle intermediate states either to diffraction or non-diffraction. Looking for connections between these contributions, let us start from an ideal exchange degenerate scheme where their separation is clear.

Some of the amplitudes possess an imaginary part Im P entirely diffractive (pp, K^+p, ... , denoted by index 2), whereas the s-u crossed ones are non-exotic (pp, K^-p, ... , denoted by index 1):

$$\mathrm{Im}\, M_2 = \mathrm{Im}\, P$$

$$\mathrm{Im}\, M_1 = \mathrm{Im}\, P + 2\, \mathrm{Im}\, N^- .$$

Our basic hypothesis is the following: the effect of the non-diffractive amplitude Im N^- will not introduce a different dependence on the interaction radius R but will only modify its value, resulting in an apparent increase ΔR^2 of the interacting area between the two colliding particles.

Taking the average value of the two radii as a reference:

$$\bar{R}^2 = \frac{1}{2}\left(R_1^2 + R_2^2\right)$$

the non-diffractive contribution is given at a fixed energy s by:

$$2\, \mathrm{Im}\, N^- = \mathrm{Im}\, P\left(\bar{R}^2 + \frac{\Delta R^2}{2}\right) - \mathrm{Im}\, P\left(\bar{R}^2 - \frac{\Delta R^2}{2}\right) . \qquad (1a)$$

In order to factorize the ΔR^2 dependence, an approximation of (1a) is also introduced:

$$2\,Im\,N^- = \Delta R^2 \frac{\partial\, Im\, P(\bar{R}^2)}{\partial R^2} \,. \qquad (1b)$$

Formulae (1a) and (1b) will be considered as the finite difference and differential forms, respectively, of our basic assumptions.

A typical property of these formulae is the expected peripheralism of Im N^-, obtained when the edge of the impact parameter profile of the Pomeron, $P(R^2,b)$ only moves with R^2. This is the case of all models satisfying GS[3], for which

$$P(R^2, b) = F(b^2/R^2) \,.$$

Consider the example of the optical model. Starting from an impact parameter profile

$$P(R^2, b) = i\, e^{-b^2/R^2} \quad or \quad i\theta(1 - b^2/R^2)$$

where θ is the step-function, ensuring a smooth or sharp cut-off at $b \equiv R$, one gets

$$Im\, P = sR^2 e^{R^2 t/4} \quad or \quad sR\, J_1(R\sqrt{-t})/\sqrt{-t} \qquad (2)$$

and consequently

$$\frac{2\, Im\, N^-}{s\,\Delta R^2} = \left(1 + \frac{\bar{R}^2 t}{4}\right) e^{\bar{R}^2 t/4} \quad or \quad J_0(\bar{R}\sqrt{-t}) \,.$$

When $\bar{R}$ is around 1 fermi, the peripheral character is evident. The different energy behaviour of the two sides of Eqs. (1) can be taken into account by a decrease of ΔR^2.

At fixed transfer it is always possible to define an appropriate change of variable $[s \leftrightarrow R(s)]$ such that Eqs. (1) are verified. *But the dynamical non-trivial hypothesis is to identify the function R(s) with the interaction radius R.* In particular, these relations cannot be reduced to a crossing property between particle and antiparticle elastic scattering.

2.2 The pratical case: negative signature amplitudes

In the following we shall focus our attention on Eq. (1b):

$$Im\, N^-(s,t) = \frac{\Delta R^2}{2} \frac{\partial\, Im\, P(\bar{R}^2, t)}{\partial R^2} \,. \qquad (3)$$

Observables for elastic reactions are defined by

$$\frac{d\sigma}{dt} = \frac{|M(s,t)|^2}{16\pi}$$

and

$$\sigma_{Tot} = Im\, M(s,0) .$$

In the following we shall neglect s-channel helicity flip amplitudes.

Im N^- is deduced from $p^{\pm}p$, $K^{\pm}p$ and $\pi^{\pm}p$ elastic reactions with the usual approximations[7,8]. A reasonable estimate of the right-hand side needs a good knowledge of R^2 and of the Pomeron dependence on it.

Except in the case of an exponential diffraction peak [for which Eq. (2) states that if $d\sigma \sim e^{Bt}$, $B = R^2/2$], there is no unambiguous way to define the radius. In order to take into account the bulk of the diffraction peak we consider the slope value averaged over a large transfer range $0 \lesssim t \lesssim 1$ GeV^2. This choice allows a realistic cut-off in the partial waves. The very forward slopes, appreciably higher than the mean ones, are more dependent on the tail properties of impact parameter distributions. Everywhere in the following, we shall identify $R^2/2$ with the effective slope B. Data are shown in Fig. 1 for $p^{\pm}p$, $K^{\pm}p$, and $\pi^{\pm}p$ elastic reactions.

Figure 1 illustrates how ∂ Im P/∂B can be determined. In the ISR energy range secondary contributions of non-diffractive events can be neglected, and since the B slope rises logarithmically with energy, one can replace ∂ Im P/∂B by ∂ Im M/∂ ln s with a good accuracy. Moreover, non-diffractive effects being probably much smaller in exotic channels, we extend this approximation to the Fermilab energy domain for pp and K^+p scattering. Thus the radius dependence is replaced by an energy dependence.

Let us consider an energy s , where Im N^-(s,t) is experimentally well known (cf. inset Fig. 1). The averaged value $\bar{B}$ of the $p^{\pm}p$ slopes at this energy are given by the shaded area of Fig. 1. Following (3) the quantity ∂ Im P/∂B must be determined at a high energy $\bar{s}$, where the pp slope reaches the mean value $\bar{B}$. The shift in energy is large enough to draw an interesting consequence: Eq. (3) relates non-diffractive and diffractive components of elastic scattering at rather different energies where they are easily distinguishable.

This relation takes a particular simple and interesting form at t = 0, thanks to the optical theorem:

$$\frac{\Delta\sigma}{\Delta B}(s_o) = \frac{\partial\sigma_P}{\partial B}(\bar{s}) \qquad (4)$$

where $\Delta\sigma(s_0)$ and $\sigma p(\bar{s})$ are, respectively, the difference between total cross-sections for anti-particle and particle scattering on protons at the energy s_0 and the Pomeron contribution at the energy $\bar{s}$ (cf. inset Fig. 1). Thus the left-hand side ratio of (4), typical of non-diffractive scattering, is related to the cross-section side at high energy.

The quantity $\partial\sigma/\partial B$ is taken as a constant λ for $p_{lab} \gtrsim 50$ GeV/c. Clearly demonstrated in the context of GS [9] for the very forward slopes, this property is also valid for averaged slopes over the whole diffraction peak. This provides us with the right-hand side of (4). Exact parametrizations are given in Table 1 without error, since this quantity is better determined than ΔB. In Fig. 2 the experimental differences ΔB are compared with the function

$$\Delta\sigma / \frac{\partial\sigma}{\partial B} = \Delta\sigma/\lambda$$

obeying a power law in energy. In order to give an idea of uncertainties, two different parametrizations have been chosen[10,11] and collected in Table 2.

Relation (4) holds remarkably well for $p^{\pm}p$ and $K^{\pm}p$ scattering down to low energies; in particular, the ΔB energy behaviour is exactly comparable to those of $\Delta\sigma$ in agreement with our conjecture.

Results are less convincing for $\pi^{\pm}p$ scattering where large experimental errors and uncertainties obscure the situation. In particular, our choice of shapes is slightly arbitrary in this reaction (for instance, there is a large discrepancy between the works of Akerlof et al.[12] and the Fermilab Single Arm Spectrometer Group[13] at p_{lab} = 100, 200 GeV/c; cf. Fig. 1) and results must be considered as only indicative in this case.

Some years ago, Kaidalov[14] showed that data on elastic processes in the forward direction supported a fixed energy relation such that

$$\sigma_1/B_1 = \sigma_2/B_2 = \Delta\sigma/\Delta B \,.$$

The analogy with the forward relation (4) deserves some comments.

i) The Kaidalov relation implies exact peripheralism in the sens that odd-crossing amplitudes, vanish at b = 0 in slight contradiction with πN amplitude analysis[15] for instance.

ii) The exact equivalence is obtained when GS is assumed, since then σ/B = constant, but GS is true only at very high energies, doubtful at lower ones[16,17] [compare with the validity range of relation (4)].

Equation (3) can also be confronted with experiment in the non-forward direction. The non-diffractive contribution N^- is obtained from differential cross-sections $d\sigma_1$ and $d\sigma_2$:

$$Im\, N^-(s,t)/\sqrt{16\pi} = \Delta d\sigma/\sqrt{8(d\sigma_1 + d\sigma_2)} \qquad (5)$$

where $\Delta d\sigma = d\sigma_2 - d\sigma_1$. The right-hand side of (3) can be expressed in terms of very high energy differential cross-sections $d\sigma_{as}$, neglecting real part and possible change of sign:

$$Im\, P(s,t)/\sqrt{16\pi} \simeq \sqrt{d\sigma_{as}}\,. \qquad (6)$$

Thus (3) becomes

$$\Delta d\sigma/\sqrt{8(d\sigma_1 + d\sigma_2)} = \frac{\Delta B}{2}\,\frac{\partial\sqrt{d\sigma_{as}}}{\partial \ln s}\left(\frac{\partial B}{\partial \ln s}\right)^{-1}. \qquad (7)$$

The left-hand side of (7) is taken from an Argonne experiment[7] and the other side from ISR results:

$$\frac{\partial\sqrt{d\sigma_{as}}}{\partial \ln s} = (\alpha_{eff} - 1)\sqrt{d\sigma_{ISR}}\,. \qquad (8)$$

The ISR effective trajectory has already been determined[18]. However we prefer to use a more recent and accurate determination[19] over all the available t-range ($0 \lesssim |t| \lesssim 4.2$ GeV^2). In Fig. 3 these two trajectories are compared and found to be well compatible. The quantity $\sqrt{d\sigma_{ISR}}$ is taken at the mean energy of the ISR range, $\sqrt{s}$ = 33.8 GeV, from an interpolation of all available results. In Fig. 4 are shown jointly the non-diffractive part of the relation (7) at p_{lab} = 5 GeV/c (full symbols) and the diffractive one (open symbols). The two data sets reflect the peripheral behaviour of both the imaginary part of odd-crossing amplitudes[4] and the Pomeron increase with energy[20]. A quantitative agreement is not reached: the position of zeros is not the same and the magnitude of effect (such as the ratio of the first to second extremum) is different. Nevertheless, it must be emphasized that energies considered do not correspond to the ones related by our scheme. Figure 1 shows that the 5 GeV/c domain for the

odd crossing amplitudes is linked with the Pomeron at 100 GeV/c, an energy where it is not available in a model independent way. We do not intend here to enter into a detailed and quite hazardous analyse of (7), but postpone the discussion to Section 3, where a complementary approach based on dual geometrical models will be presented.

2.3 Exchange degeneracy breaking

Up to now we have restricted ourselves to the study of odd-crossing distributions. Let us explain how other exchanges enter into the scheme. There are many arguments against strong exchange degeneracy. The study of inelastic reactions seems to indicate that even-crossing contributions are not peripheral[21]. In fact our conjecture implies an exchange-degeneracy breaking and a well-defined extrapolation of the Pomeron at non-asymptotic energies. Denoting the energies where the slopes of the diffraction peaks B_2 and B_1 are equal (cf. inset of Fig. 1) as s_0 and s_1, respectively, the finite difference form (1a) becomes

$$2\,\mathrm{Im}\,N^{-}(s_0,t) = \mathrm{Im}\,P(s_1,t) - \mathrm{Im}\,P(s_0,t)\,. \qquad (9)$$

This equation defines the Pomeron at the intermediate energy s_0: $\mathrm{Im}\,N^{-}(s_0,t)$ is given by the difference of elastic differential cross-sections and $\mathrm{Im}\,P\,(s_1,t)$ deduced from asymptotic energies.

Now let us concentrate on the forward direction. At high energies ($p_{lab} \gtrsim 100$ GeV) the Pomeron grows like the slope of the diffraction peak B_1 [9]:

$$\sigma_P\,(s_1) = \lambda\, B_1\,(s_1) \qquad (10)$$

where λ is the constant ratio σ/B (cf. Table 1). However, since our starting hypothesis is based on a fonctional dependence of amplitudes on the Pomeron interaction radius, it is legitimate to extend Eq. (10) to the whole energy domain, and straightforward to show that Eqs. (1a) and (1b) become identical:

$$\Delta\sigma\,(s_0) = \sigma_P\,(s_1) - \sigma_P\,(s_0) = \lambda\, B_1\,(s_1) - \lambda\, B_1\,(s_0)\,.$$

One must be aware of approximations used. In particular, these remarks rely on the assumption that contrary to other observables, the mean slopes $B_1(s)$ are not too sensitive to violation of exchange degeneracy since the Pomeron slope is inferred from the exotic process.

Incidentally let us point out that, though our study of πN scattering is not very conclusive (in fact the situation is obscured by technical difficulties such as precise determination of forward slope differences, the lack of exoticity

arguments, etc.) an even worse situation could have occur: in πN scattering and contrary to other reactions, the mean slope value $\bar{B}$ stays in the non-asymptotic energy domain (cf. Fig. 1). The πN ratio $\partial\sigma/\partial B$ is no longer constant and even could be negative since $\pi^{\pm}p$ total cross-sections decrease simultaneously when the slopes increase[22]. Thus one would obtain negative values for the right-hand side of (4). The former discussion gives another argument in support of the high-energy constant value $\partial\sigma/\partial B$, experimentally valid only above 100 GeV/c, but extrapolated to lower energies through the Pomeron contribution.

From standard decomposition of amplitudes, we easily derive the imaginary parts C^+ and C^- of odd and even signature contributions in the forward direction:

$$C^+(s) - C^-(s) = \sigma_1(s) - \lambda B_1(s)$$

$$C^+(s) = \sigma_1(s) - \lambda B_1(s) + \frac{1}{2}\Delta\sigma(s) \,.$$

In order to illustrate these remarks we have plotted in Fig. 5 the total cross-sections for pp $[\sigma_T(pp)]$ and $\bar{p}p$ $[\sigma_T(\bar{p}p)]$ together with the central values of the slopes rescaled by the λ-factor. The approximate equality of shaded areas down to quite low energies is another way to ascertain the validity of relation (4). A strong exchange-degeneracy breaking is obtained, since for instance the Pomeron contributions to $\sigma_T(pp)$ is 30 mb only at 7 GeV/c. This characteristic feature and the linearly increase with log s of the Pomeron contribution are quite similar to recent results[23] obtained through a perturbative approach to Reggeon calculus.

3. A GEOMETRICAL MODEL FOR THE POMERON FROM NON-DIFFRACTIVE PROCESSES

3.1 Inducing the Pomeron from s-channel models of non-diffractive reactions

From the above discussion rather convincing phenomenological arguments support the geometrical relation. Here we wish to obtain a better understanding of diffractive amplitudes from geometrical studies of non-diffractive ones through this relation:

$$Im\, N^-(s_0,t) = K \frac{\partial\, Im\, P(\bar{s},t)}{\partial \ln(s)} \qquad (11)$$

where we recall that K is the following function of energy:

$$K = \Delta B(s_0)/2 \frac{\partial B}{\partial \ln s}(\bar{s}) \qquad (12)$$

s_0 and $\bar{s}$ are again defined by the energy shift sketched in Fig. 1. Two models have popularized geometrical ideas: in the dual absorption model of Harari[4] (DAM) imaginary parts of negative signature non-flip amplitudes possess a very simple peripheral structure:

$$Im\, N^-(s,t) \propto J_0(R\sqrt{-t}) \tag{13}$$

where J_0 is the zeroth-order Bessel function and R is around 1 fermi. In the dual peripheral model of Schrempp and Schrempp[5] (DPM) a very successful extension of DAM is given by the parametrization:

$$Im\, N^-(s,t) = Im\left[i\, A(s)\, \mathcal{H}_0\left(b_0(s)\sqrt{-t}\right)\right] \tag{14}$$

where $\mathcal{H}_0$ is the Hankel function of the first kind. Note that this model is not valid in the very forward direction. Now the interaction radius $b_0(s)$ is a complex number and A(s) an unknown residue function. The radius controls both the peripheral structure by its imaginary part and the exponential fall-off by its real part, since an approximation of the Hankel function, valid already[5] at $-t \gtrsim 0.25\ GeV^2$ shows clearly:

$$Im\, N^-(s,t) \simeq (-t)^{-1/4}\, e^{-Im\, b_0(s)\sqrt{-t}} \cos\left(Re\, b_0(s)\sqrt{-t} - \varphi(s)\right). \tag{15}$$

Moreover, since the function A(s) is expected to be approximately real at moderate energies, the phase $\phi(s)$ is quite similar to the Hankel-function one:

$$\varphi(s) \simeq \frac{\pi}{4} + \frac{1}{2}\arctg\left(Im\, b_0(s)/Re\, b_0(s)\right).$$

This model appears firmly predictive and has been successfully tested on inelastic reactions[5].

From the preceding section, we have some reason to hope that the quantity $\partial\, Im\, P/\partial\, \ln s$ has something to do with the parametrizations (13) and (14). At small t we already checked that the related experimental quantity (8) has a peripheral structure (cf. Fig. 4). In the same figure this quantity together with its non-diffractive counterpart *is described by the same functional dependence* given by DPM:

$$K(\alpha_{eff} - 1)\sqrt{d\sigma_{ISR}} = 9.68\ mb^{1/2}\, GeV^{-1}\ Im\left[i\, \mathcal{H}_0\left(b_0^D(s)\sqrt{-t}\right)\right] \tag{16}$$

$$\Delta d\sigma / \sqrt{8(d\sigma_1 + d\sigma_2)} = 2.8\ mb^{1/2}\ GeV^{-1}\ Im\left[i\,\mathcal{H}_0\left(b_0^{ND}(s)\sqrt{-t}\right)\right] \qquad (17)$$

with $b_0^D(s) = 5.1 + i\ 3.71\ GeV^{-1}$, whereas the radius obtained from the non-diffractive contribution at 5 GeV/c [7] is $b_0^{ND}(s) = 6 + i\ 1.05\ GeV^{-1}$.

These fits illustrate the mechanism of relation (11): the two related quantities have the same functional forms, but with different values of interaction radii. Real parts are both near 1 fermi, as is expected from non-diffractive s-channel trajectory properties[5]. Imaginary parts differ strongly but, in contradistinction to the real parts, are known to vary rapidly with energy[5]. Thus the shift in energy inherent to such a comparison should be attributed to them. Our lack of knowledge on the Pomeron trajectory and on the non-diffractive peripheral trajectory at very high energy impedes us from going further.

In Fig. 6 we have plotted $(-t)^{1/4}\ \partial\sqrt{d\sigma}/\partial \ln s$ as a function of $\sqrt{-t}$ and compared with the approximation of the Hankel function:

$$(-t)^{1/4}\ \frac{\partial\sqrt{d\sigma}}{\partial \ln s} = .6\ mb^{1/2}\ GeV^{-1/2}\ e^{-3.71\sqrt{-t}} \cos\left(5.1\sqrt{-t} - 1.1\right) \qquad (18)$$

where the $\sqrt{-t}$ exponential behaviour modulated by an oscillating function is exhibited. Also we tried a Bessel function J_0 fit[4]. Figure 7 compares the two DAM and DPM results. The exponential fall-off in square root of the transfer variable is clearly favoured up to the largest t-values.

3.2 A geometrical description of the Pomeron

In order now to get the Pomeron amplitude, we are faced with the problem of integrating relations like (16) or (18). The main difficulty lies in our ignorance of the energy behaviour of parameters. In particular the s-dependence of $b_0^D(s)$, the "s-channel singularity" of the Pomeron, cannot be inferred from non-diffractive processes. Thus we present an inductive solution, in good agreement with ISR data, to be chosen among the family of solutions suggested by Eq. (18):

$$\mu(\xi, \sqrt{-t})\ Im\ P(s,t) \simeq e^{-a(\xi)\sqrt{-t}} \sin\left(\beta(\xi)\sqrt{-t} + \psi(\xi)\right) \qquad (19)$$

where μ, a, β and ψ can depend on $\xi = \ln s$.

From a phenomenological point of view we expect that the experimental quantities $\sqrt{d\sigma_{as}}$ corrected by an appropriate factor, share the same properties as $(-t)^{1/4}\,\partial\sqrt{d\sigma_{as}}/\partial\xi$ namely, an exponential fall-off and regular oscillations in $\sqrt{-t}$ (remember Fig. 6).

The -- somewhat arbitrary but successful -- choice of the $\sqrt{-t}$ dependence of the μ factor was made by analogy with the simplest optical model [cf. Eq. (22)], where

$$\frac{\partial\, Im\, P}{\partial R^2} \Big/ Im\, P = J_0(R\sqrt{-t}) \Big/ \left(\frac{R J_1(R\sqrt{-t})}{\sqrt{-t}}\right) \simeq \sqrt{-t} \times \text{oscillations}$$

and from Eq. (18):

$$\mu(\xi, \sqrt{-t}) \simeq (-t)^{3/4} .$$

The quantity $(-t)^{3/4}\sqrt{d\sigma}$ is shown in Fig. 8 for all available ISR energies. Some striking regularities emerge immediately:

- an exponential fall-off in $\sqrt{-t}$ exactly comparable with those of the derivative (compare Figs. 6 and 8),
- regular oscillations in $\sqrt{-t}$ of larger period than in the derivative amplitude; in fact the real part of the radius is roughly reduced by half (i.e. ~ 0.5 fermi) in comparison with the previous one.

These characteristics must be precisely stated in order to provide a quantitative description of ISR data. Our reasoning is mainly based on the presence of a zero in the imaginary part of the Pomeron amplitude near $|t| \simeq 1.4\ \text{GeV}^2$, appearing clearly as a sharp minimum in Fig. 8. This allows one to explain this strong breaking of the universality of the hadron radius and to determine the parameters of Eq. (19).

The argument is the following: it turns out that $\partial\sqrt{d\sigma}/\partial\xi$ contains the zeros of both Im P and ∂ Im P/$\partial\xi$, since we have:

$$\sqrt{d\sigma} \simeq |Im\, P| = \varepsilon\, Im\, P$$

and

$$\frac{\partial\sqrt{d\sigma}}{\partial\xi} \simeq \varepsilon\, \frac{\partial\, Im\, P}{\partial\xi}$$

where ε is the sign of Im P. Then a zero of Im P induces a discontinuity in $\partial\sqrt{d\sigma}/\partial\xi$, which becomes a sharp dip when secondary effects (real part, flip

amplitudes) are considered. The above mentionned zero in Fig. 8 can be seen also in $\partial \sqrt{d\sigma}/\partial\xi$ (cf. Fig. 7). The origin of the doubled period in $(-t)^{3/4} \sqrt{d\sigma}$ becomes clear: one of the zeros of $(-t)^{1/4} \partial \sqrt{d\sigma}/\partial\xi$ is not a zero of ∂ Im P/$\partial\xi$ but the reflection of a zero of Im P itself.

To be more precise, let us factorize the expression (18):

$$\frac{\partial \sqrt{d\sigma}}{\partial \xi} \propto e^{-3.71\sqrt{-t}} \sin(2.55\sqrt{-t} + .235) \cos(2.55\sqrt{-t} + .235) \qquad (20)$$

and assign a zero of the sine function to Im P and a zero of the cosine function to ∂ Im P/$\partial\xi$. Extending this factorization to all the t-range (except $|t| \lesssim 0.25$ GeV^2) -- here is the strong approximation of the derivation -- and referring to the general solution (19) we obtain

$$\mathrm{Im}\, P(s,t) = g\,(-t)^{-3/4}\, e^{-a(\xi)\sqrt{-t}} \sin(\beta(\xi)\sqrt{-t} + \psi(\xi)) \,. \qquad (21)$$

The averaged values of the parameters $a(\xi)$, $\beta(\xi)$, and $\psi(\xi)$ suggested by the factorization (20) are

$$a(\xi) \simeq 3.71\ \mathrm{GeV}^{-1} \;;\; \beta(\xi) \simeq 2.55\ \mathrm{GeV}^{-1} \;;\; \psi(\xi) \simeq .23. \qquad (22)$$

Then if ∂ Im P/$\partial\xi$ is proportional to $\cos[\beta(\xi)\sqrt{-t} + \psi(\xi)]$, the parameters g and $a(\xi)$ must be energy independent. One then writes

$$(-t)^{3/4} \frac{\partial \mathrm{Im}P}{\partial \xi} = g\, e^{-a\sqrt{-t}} \cos(\beta(\xi)\sqrt{-t} + \psi(\xi)) \left(\frac{d\beta}{d\xi}\sqrt{-t} + \frac{d\psi}{d\xi}\right) \qquad (22)$$

and

$$\alpha_{eff} - 1 = \mathrm{ctg}[\beta(\xi)\sqrt{-t} + \psi(\xi)] \left(\frac{d\beta}{d\xi}\sqrt{-t} + \frac{d\psi}{d\xi}\right) \,. \qquad (23)$$

The corresponding fits are shown in Figs. 3 and 8. Some comments are in order:

i) The predicted energy independence of parameters g and $a(\xi)$ is clearly confirmed by the existence of a universal straight line tangent to all data in

Fig. 8. Moreover, the parameter $a(\xi)$ is identical to Im b_0^D deduced from the fit of $\partial \sqrt{d\sigma}/\partial \ln s$, namely 3.71 GeV^{-1}.

ii) The oscillations are correctly reproduced for $\sqrt{-t} \gtrsim 0.5$ GeV. Discrepancies for lower values are expected since the validity of the DPM model and therefore of the functions we started with are subject to this restriction[5].

Parameters obtained are listed in Table 3. A global solution is reached with the constant value 2.55 GeV^{-1} for the radius real part $\beta(\xi)$ deduced from the study of $\partial \sqrt{d\sigma}/\partial \ln s$. The corresponding effective trajectory is plotted in Fig. 3. The derivative $d\psi/\partial\xi$ which enters into Eq. (23) is computed from the extremum values of the fit and the ψ value chosen is the average of these numbers.

The remaining problem is the inconsistency of the initial geometrical picture. If Eq. (11) is true, Im N^- and ∂ Im $P/\partial\xi$ have similar t-dependence, allowing for possible alteration due to the energy shift from s_0 to $\bar{s}$. Quite to the contrary, the phenomenological analysis has shown that the scales which govern the zero spacing are strongly different: near 1 fermi for Im $N^{(-)}$ but ½ fermi for ∂ Im $P/\partial\xi$. (Incidentally note that this does not involve the first "peripheral" zero of both functions but arises from the existence of the second one.) We have no satisfactory answer to this puzzle but let us put forward two possible conjectures:

i) The geometrical relations is valid only at a functional level: non-diffractive and diffractive scattering are qualitatively connected through geometrical variables, but not quantitatively to the extent that b_0^D is not directly related with b_0^{ND}.

ii) The geometrical relation involves the quantity $\sqrt{d\sigma}$ and not the imaginary parts of the amplitude. Then the equality of geometrical scales for non-diffractive and diffractive processes is recovered. Our quantitative results would not change since there is essentially difference between $\sqrt{d\sigma_1} - \sqrt{d\sigma_2}$ and $\Delta\sigma/\sqrt{d\sigma_1 + d\sigma_2}$.

In spite of its limitations, the solution we found is satisfactory enough to reveal the simple geometrical properties of the Pomeron. As a final illustration we have plotted in Fig. 9 the differential pp cross-section at the mean ISR energy (p_{beam} = 26.7 GeV/c) as a function of t. Oscillations in $\sqrt{-t}$ reproduce the dip structure and the property of tangency to a curve proportional to $(-t)^{-3/2}\, e^{-7.42\sqrt{-t}}$ is nicely illustrated.

3.3 On s- and t-channel interpretations of our parametrization

In this section, we discuss some theoretical questions raised by the solution we find for the Pomeron derivative with respect to energy [Eq. (18)] and its approximate integrated form [Eq. (22)]. The DPM formulation corresponds to a complex pole in the impact parameter plane:

$$F_{DPM}(b,s) \simeq Im \frac{1}{b^2 - b_o^2(s)} . \tag{24}$$

From duality arguments the peripherality of this model is inferred from the peripheral character of resonances, embodying the Harari ansatz[4]. Now a first question concerns the compatibility of this s-channel property of $\partial \sqrt{d\sigma/\partial\xi}$ with the idea of GS, which means a special behaviour of the diffractive amplitude

$$\sqrt{d\sigma}(b) = f(b^2/R^2)$$

and of its derivative

$$\frac{\partial \sqrt{d\sigma}(b)}{\partial \xi} = -\frac{b^2}{R^4} f'(b^2/R^2) \frac{\partial R^2}{\partial \xi} .$$

Since the slope is compatible with a ln s dependence[9] ($R^2 = R_0 + \gamma\xi$) we have

$$\frac{\partial \sqrt{d\sigma}}{\partial \xi}(b) = (\gamma R^2)^{-1} \phi(b^2/R^2) \tag{25}$$

where $\phi(x) = -x f'(x)$.

Equations (25) must be compared with Eq. (16) translated into the b-space

$$\frac{\partial \sqrt{d\sigma}}{\partial \xi} \simeq Im\left[b_o^{-2} (b^2/b_o^2 - 1)^{-1} \right] . \tag{26}$$

Ignoring extra s-dependence, our solution can be related to a geometrical scaling in the complex radius b_0^2 instead of R^2. The question whether a supplementary energy dependence exists or not is unsolved as well as the more

general problem of the s-channel trajectory $b_0^2(s)$. For instance, the approximate solution we find [Eq. (22)] does not verify explicitly GS. Nevertheless, a lesson can be drawn from a general solution of Eq. (26):

$$\sqrt{d\sigma}(b) = Im\left[\int_{b_m}^{b_0^2(\xi)} \frac{\omega(x)}{b^2 - x}\, dx\right] \tag{27}$$

where b_m is a constant and $\omega(x)$ an unknown function. Differentiating (27) with respect to ξ gives

$$\frac{\partial \sqrt{d\sigma}}{\partial \xi}(b) = Im\left[\omega(b_0^2)\, \frac{\partial b_0^2}{\partial \xi}\, (b^2 - b_0^2)^{-1}\right] \tag{28}$$

which is compatible with (26) when $\omega(b_0^2)\partial b_0^2/\partial\xi$ is real.

Solution (27) is nothing else than a cut definition in the impact parameter plane with a moving end point $b_0(\xi)$ and a discontinuity given by $\omega(x)$. In the DPM model, high-energy non-diffractive processes are related to the s-channel resonances which must lie on a trajectory $b^2_{resonance}$. If (27) has something to do with reality, the Pomeron would be dual to an s-channel cut with an end point b^2_{cut}, in nice agreement with topological properties of duality diagrams contributing respectively to Regge poles and the Pomeron[1]. Consequently, our geometrical picture says that vector Regge poles and the Pomeron derivative share the same functional dependence -- complex poles in the impact parameter plane -- but with different values of the trajectory. The non-diffractive one is connected with s-channel resonances, but the diffractive trajectory would correspond to low-energy singularities of the cut type.

A t-channel interpretation of such results is not clear at first sight since, up to now, all our discussion is based on direct-channel considerations. However, an answer may be found in the papers of Anselm and Dyatlov[24] where, from a t-channel approach, similar parametrizations are deduced:

$$\begin{aligned} Im\, P(s,t) &= F_1(\xi, \sqrt{-t})\, e^{-R_1(\xi)\sqrt{-t}} \cos\left(R_2(\xi)\sqrt{-t} + \varphi_0(\xi, \sqrt{-t})\right) \\ \frac{\partial\, Im\, P(s,t)}{\partial \xi} &= F_2(\xi, \sqrt{-t})\, e^{-R_1(\xi)\sqrt{-t}} \cos\left(R_2(\xi)\sqrt{-t} + \tilde{\varphi}_0(\xi, \sqrt{-t})\right). \end{aligned} \tag{29}$$

where F_1, F_2, ϕ_0, and $\tilde{\phi}_0$ are smoothly varying function of $\sqrt{-t}$. This family of solutions contains without modification our set (22) with a particular choice of the unknown functions in (29). The t-channel ingredient used by the authors of Ref. 24 is the accumulation of Mandelstam branch-points, i.e. n-Reggeon exchange cuts. They show that away from the very forward direction the high n cuts would dominate the scattering. These results do not depend strongly on the detailed dynamical structure of cut discontinuities except for a crucial $(-1)^n$ factor due to t-channel unitarity conditions. This interpretation leads us to conclude that typical effects of accumulation of n-Reggeon cuts alternating in sign are present already at small momentum transfer in the ISR range. The fact that such effects can play a role up to the highest momentum transfer values incites us to draw a parallel with analysis of large p_T elastic reactions[6,25,26], where parametrizations of type (29) are used. While a detailed comparison would be instructive, the similarity of the parameters found in Ref. 25 and in this work is quite encouraging.

4. SUMMARY AND OUTLOOK

From a simplified picture of elastic scattering, we conclude that non-diffractive amplitudes (odd signature imaginary part) and diffractive ones (energy derivative of the Pomeron) have a related functional dependence on their geometrical characteristics, namely the complex radius of interaction. Phenomenological support for this view comes from the following:

i) The ratio of differences of total cross-sections to diffraction-peak slopes for s-u crossed reactions scales at all energy to the value of the asymptotic rise of cross-sections with ln s (clearly true for $p^{\pm}p$ and $K^{\pm}p$ scattering, more doubtful for $\pi^{\pm}p$).

ii) The same function, up to a change in the complex radius, describes the odd signature contribution in pp scattering at p_{lab} = 5 GeV/c and the asymptotic quantity deduced from ISR data $\partial \sqrt{d\sigma}/\partial \ln s$.

A new geometrical picture of the Pomeron emerges with the following interesting characteristics:

i) The appearance of one length scale of order 0.5 fermi.

ii) Large oscillations and a universal exponential cut-off, both in terms of the variable $\sqrt{-t}$.

From the initial geometrical relation, verified at zero transfer, we kept only the functional dependence between non-diffractive and diffractive related parts. The difference of scale between these components remains a little mysterious.

The knowledge of the s-channel trajectory of the Pomeron would be a crucial step towards a better understanding of this phenomena. This could lead, in particular, to an explicit relation between the Pomeron shrinkage and those of other Reggeons.

Finally, let us mention some possible development:

i) The connection with Gribov calculus suggested by results of Ref. 23 needs a thorough study.

ii) The similarity of our results with recent analyses at large p_T [25,26] suggests that geometrical ideas control a large domain in energy and transfer, irrespective of properties of inner constituents of the hadronic matter. However, note that the question of whether there is any indication of internal structure in two-body strong interactions is open. This would imply a kind of geometrical universality between all elastic channels[33].

After completing this work, we learned that some geometrical aspects of elastic scattering have been studied using the Fermilab data, in the framework of GS [34]. The results quoted are in agreement with our starting hypothesis (Section 2.1). Our analysis shows that geometrical properties are quite general and valid in a large domain of energy and transfer.

Acknowledgements

We are particularly indebted to Alexander Martin for providing us with his most recent analysis of ISR data. We are also very grateful for clarifying discussions with A. Capella, H. Cornille, G. Cohen-Tannoudji, A.B. Kaidalov, B. and F. Schrempp and other colleagues of the Service de Physique Théorique (CEA-Saclay) and of the CERN Theory Division. Furthermore we thank F. Schrempp for his critical reading of the manuscript.

REFERENCES

1) Huan-lee, Phys. Rev. Letters 30, 719 (1973).
G. Veneziano, Phys. Letters 43B, 413 (1973).
G. Cohen-Tannoudji, Herceg-Novi Summer School on Elementary Particle Physics, 1972.

2) T.T. Chou and C.N. Yang, Phys. Rev. 170, 1591 (1968); 175, 1832 (1968).

3) J. Dias de Deus, Nuclear Phys. B59, 231 (1973).
A.J. Buras and J. Dias de Deus, Nuclear Phys. B71, 481 (1974).

4) H. Harari, Ann. Phys. (NY) 63, 432 (1971).

5) B. Schrempp and F. Schrempp, Nuclear Phys. B54, 525 (1973); B60, 110 (1973); B77, 453 (1974).

6) B. Schrempp and F. Schrempp, Rapporteur's talk at the EPS Internat. Conf. on High-Energy Physics, Palermo, 1975, to be published in the Proceedings.

7) I. Ambats et al., Phys. Rev. Letters 29, 1415 (1972); Phys. Rev. D9, 1179 (1974).

8) G. Brandenburg et al., Phys. Letters 58B, 367 (1975).

9) V. Barger, J. Luthe and R.J.N. Phillips, Nuclear Phys. B88, 237 (1975).

10) V. Barger, Proc. 17th Internat. Conf. on High-Energy Physics, London, 1974 (Rutherford Lab., Chilton, Didcot, 1974), p. I.205.

11) A.N. Diddens, Proc. 17th Internat. Conf. on High-Energy Physics, London, 1974, p. I.41.

12) C.W. Akerlof et al., ANL-HEP-PR-75-43 and Phys. Rev. Letters 35, 1406 (1975).

13) Fermilab, Single Arm Spectrometer group, Phys. Rev. Letters 35, 1196 (1975).

14) A.B. Kaidalov, Yadernaya Fiz. 16, 389 (1972) [Soviet J. Nuclear Phys. 16, 217 (1973)].

15) H. Hogaäsen and C. Michaël, Nuclear Phys. B44, 214 (1972).

16) W. Grein, R. Guigas and P. Kroll, Nuclear Phys. B89, 93 (1975).

17) W. Grein and P. Kroll, Phys. Letters 58B, 74 (1975).

18) A. Martin, Nuclear Phys. B77, 226 (1974).
P.D.B. Collins, F.D. Gault and A. Martin, Nuclear Phys. B80, 135 (1974).

19) Alexander Martin, private communication.

20) H. Miettinen, Comptes Rendus de la 9e Rencontre de Moriond, Méribel-les-Allues, 1974 (Lab. de Phys. Théorique et Particules Elémentaires, Orsay, 1974) (Ed. J. Tran Than Van), Vol. 1, p. 363.

21) P.R. Stevens, Phys. Rev. D9, 1425 (1974).
G. Girardi, C. Godrèche and H. Navelet, Nuclear Phys. B76, 541 (1974); B83, 515 (1974).
F. Elvekjaer and R. Johnson, Nuclear Phys. B83, 142 (1974).

22) A.M. Wetherell, Invited talk at the EPS Internat. Conf. on High-Energy Physics, Palermo, 1975, to be published in the Proceedings.

23) A. Capella, J. Kaplan and J. Tran Than Van, Nuclear Phys. B97, 493 (1975).

24) A.A. Anselm and I.T. Dyatlov, Phys. Letters 24B, 479 (1967); Yadernaya Fiz. 6, 591 (1967) [Transl.: Soviet J. Nuclear Phys. 6, 430 (1968)].

25) B. Schrempp and F. Schrempp, Phys. Letters 55B, 303 (1975).

26) F. Elvekjaer and J.L. Petersen, Nuclear Phys. B94, 100 (1975).

27) T. Lasinski, R. Levi Setti, B. Schwarzschild and P. Ukleja, Nuclear Phys. B37, 1 (1972).

28) A.C. Melissinos and S.L. Olsen, Phys. Reports 17C, 96 (1975).

29) Ya.M. Antipov et al., Nuclear Phys. B57, 333 (1973) and Contribution to the EPS Internat. Conf. on High-Energy Physics, Palermo, 1975.

30) A. Böhm et al., Phys. Letters 49B, 491 (1974).
M. Holder et al., Phys. Letters 36B, 400 (1971).
U. Amaldi et al., Phys. Letters 36B, 504 (1971).
C. Barbiellini, Phys. Letters 39B, 663 (1972).

31) R.K. Carnegie et al., Phys. Letters 58B, 371 (1975).

32) N. Kwak et al., Phys. Letters 58B, 233 (1975).

33) J. Dias de Deus, Acta Phys. Polon. B6, 613 (1975).

34) J. Dias de Deus and P. Kroll (private communication by F. Schrempp).
V. Barger and R.J.N. Phillips, Rutherford Laboratory preprint RL-75-176 (December 1975).

Table 1

Asymptotic parametrization of slopes and cross-sections

$$\begin{pmatrix} B \\ \sigma \end{pmatrix} = \begin{pmatrix} B_0 \\ \sigma_0 \end{pmatrix} (1.0 + 0.068 \ln s)$$

values of B_0/σ_0 are compatible with those found by Grein and Kroll (Ref. 17).

Channel	B_0 (GeV^{-2})	σ_0 (mb)	B_0/σ_0 $(GeV^2\ mb)^{-1}$
pp	7.73	28.2	0.274
Kp	5.56	14.1	0.394
πp	5.9	16.92	0.349

Table 2

Fit parameters for the total cross-section differences:

$$\Delta\sigma = a\, E_{lab}^{-b} \quad \text{(Bartel-Diddens, Ref. 19)}$$

and

$$\Delta\sigma = c\, s^{-0.55} \quad \text{(Barger, Ref. 10)}$$

Channel	a (mb)	b	c (mb)
pp	51.66	0.575	69.6
Kp	17.76	0.531	27.1
πp	4.7	0.370	12.4

Table 3

Values of parameters describing ISR data

$g = 5.6\ \sqrt{mb}\ \sqrt{GeV}$; $\beta = 2.55\ GeV^{-1}$; $a = 3.71\ GeV^{-1}$						
P_{beam} (GeV/c)	11.5	11.8	15.4	22.4	26.7	31.5
ψ	0.12	0.125	0.145	0.18	0.20	0.285

Figure captions

Fig. 1 : Slopes of elastic diffraction peaks as functions of laboratory momentum for $0 \lesssim |t| \lesssim 0.8$ GeV^2. Open and full symbols correspond, respectively, to antiparticle and particle beams. The following data have been used:
a) $p^{\pm}p$: Ref. 27 (2, 3 GeV/c), Ref. 12 (5, 6 GeV/c), Refs. 27, 28 (9, 12 GeV/c), Ref. 29 (25, 29, 40, 43 GeV/c), Ref. 13 (50, 70, 100, 140, 175 GeV/c), Ref. 30 (ISR energies)
b) $K^{\pm}p$: Refs. 7, 31 (3, 3.65, 5, 6, 10.4, 14 GeV/c), Refs. 12, 27 (10 GeV/c), Ref. 29 (25, 29, 40, 43 GeV/c), Ref. 13 (50, 70, 100, 140, 175 GeV/c).
c) $\pi^{\pm}p$: Ref. 7 (3, 3.65, 5, 6 GeV/c), Ref. 29 (25, 29, 40, 43 GeV/c), Ref. 13 (50, 70, 100, 140, 175 GeV/c), Ref. 12 (100, 170 GeV/c).
Solid lines are asymptotic B (for details see text and Table 1), shaded areas are the mean slope values $\bar{B}$. Furthermore, in an inset, the $p^{\pm}p$ case is sketched in.

Fig. 2 : Test of the geometrical relation in the forward direction. Symbols: ■ Ref. 13; ○ Ref. 29; ● Refs. 7, 31; X Ref. 12; ⊙ Refs. 27, 28; ▲ Ref. 27.

Fig. 3 : Effective trajectory for pp scattering at ISR from Ref. 18 (full circles) and from Ref. 19 (open circles) compared with $\alpha(t) = 0.085\ \mathrm{ctg}(2.55\sqrt{-t} + 0.2)$.

Fig. 4 : Illustration of the geometrical relation up to $|t| \sim 1.3$ GeV^2. Diffractive data from ISR[30] and non-diffractive data from Ref. 7.

Fig. 5 : Predictions for non-diffractive contributions in the forward direction. Central points of elastic slopes B are rescaled by the λ factor (cf. Table 1) and reported together with total cross-sections.

Fig. 6 : The quantity $\sqrt[4]{-t}(\alpha_{eff} - 1)\sqrt{d\sigma}$ for pp scattering at 600 GeV/c [30] plotted versus $\sqrt{-t}$; Open circles for negative values and full circles for positive ones. The curve corresponds to the approximation of the Hankel function: $0.6\ e^{-3.71\sqrt{-t}} \cos(5.1\sqrt{-t} - 1.1)$. The solid line is predicted to be tangent to data.

Fig. 7 : The quantity $(\alpha_{eff} - 1)\sqrt{d\sigma}$ plotted versus t. Symbols and references same as before, but now the curve corresponds to:

$$0.6\ e^{-3.71\sqrt{-t}} \cos(5.1\sqrt{-t} - 1.1)$$

The inset presents also a DAM solution (dashed line):

$$0.434\ J_0(4.53\sqrt{-t})e^{2.62t}$$

compared to the DPM solution (solid line).

Fig. 8 : The quantities $(\sqrt{-t})^{3/2}\sqrt{d\sigma}$ are plotted versus $\sqrt{-t}$ at ISR impulsion beams (Refs. 30, 32)

a) 11.5, 11.8 and 15.4 GeV/c

b) 22.4, 26.7 and 31 GeV/c

Curves correspond to a Hankel function fit with parameters given in Table 3. The line is the predicted universal tangent $5.6\ e^{-3.71\sqrt{-t}}$.

Fig. 9 : pp differential cross-section at ISR impulsion beam 26.7 GeV/c. Regularities predicted at large momentum transfer are exhibited.

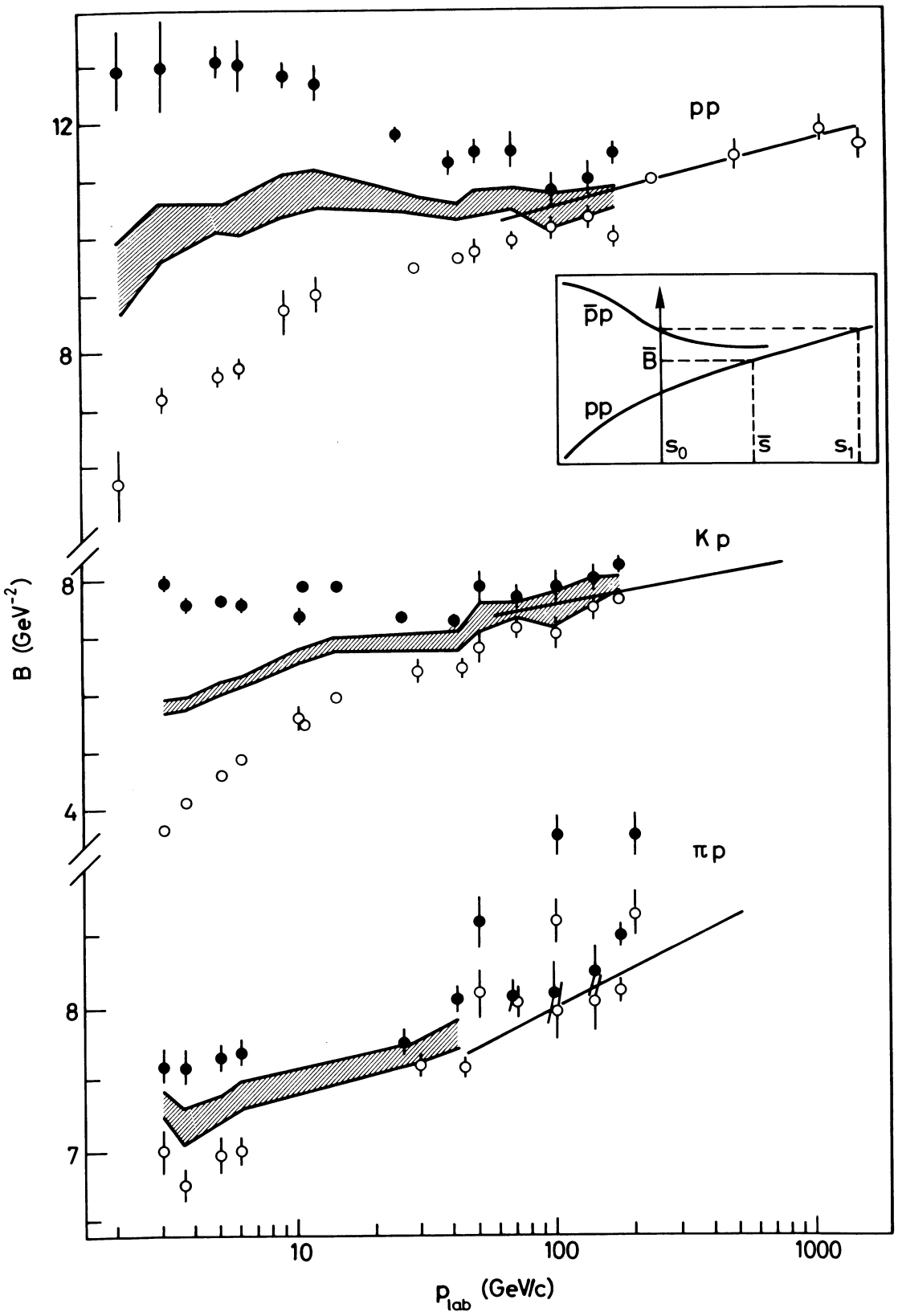

Fig. 1

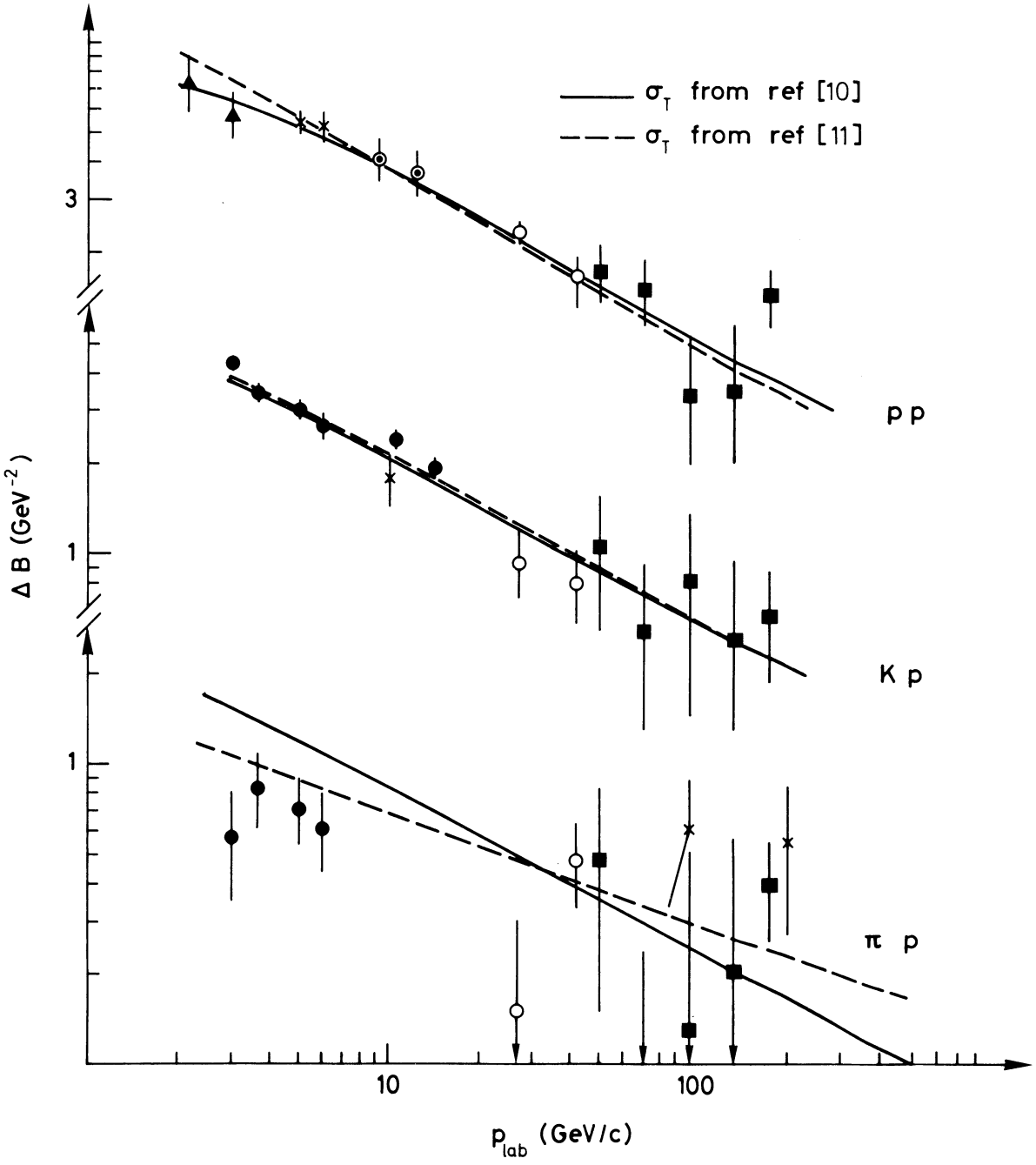
σT from ref [10]
σT from ref [11]
p p
K p
π p
3
1
1
Δ B (GeV⁻²)
10
100
p lab (GeV/c)

Fig. 2

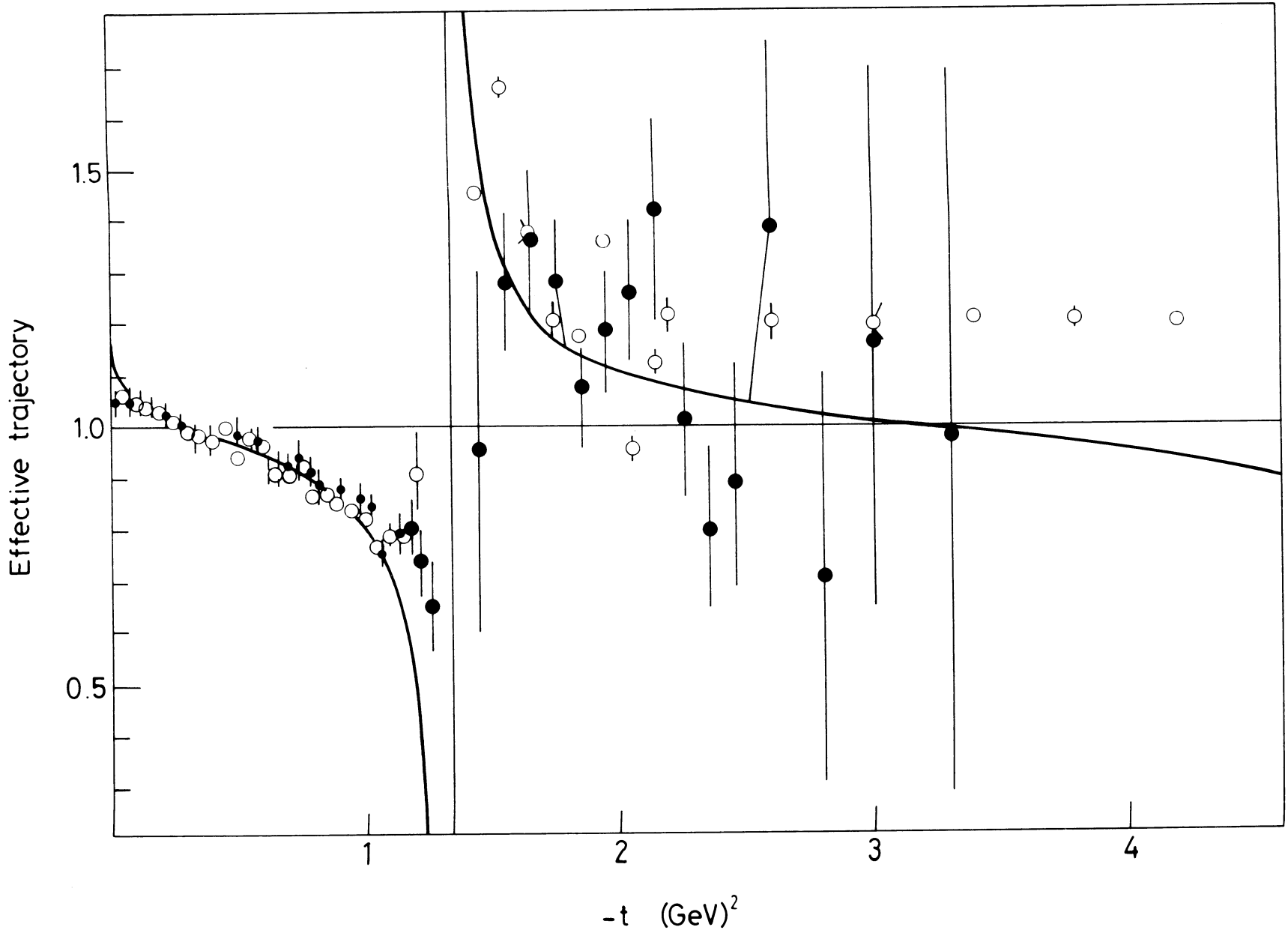

Fig. 3

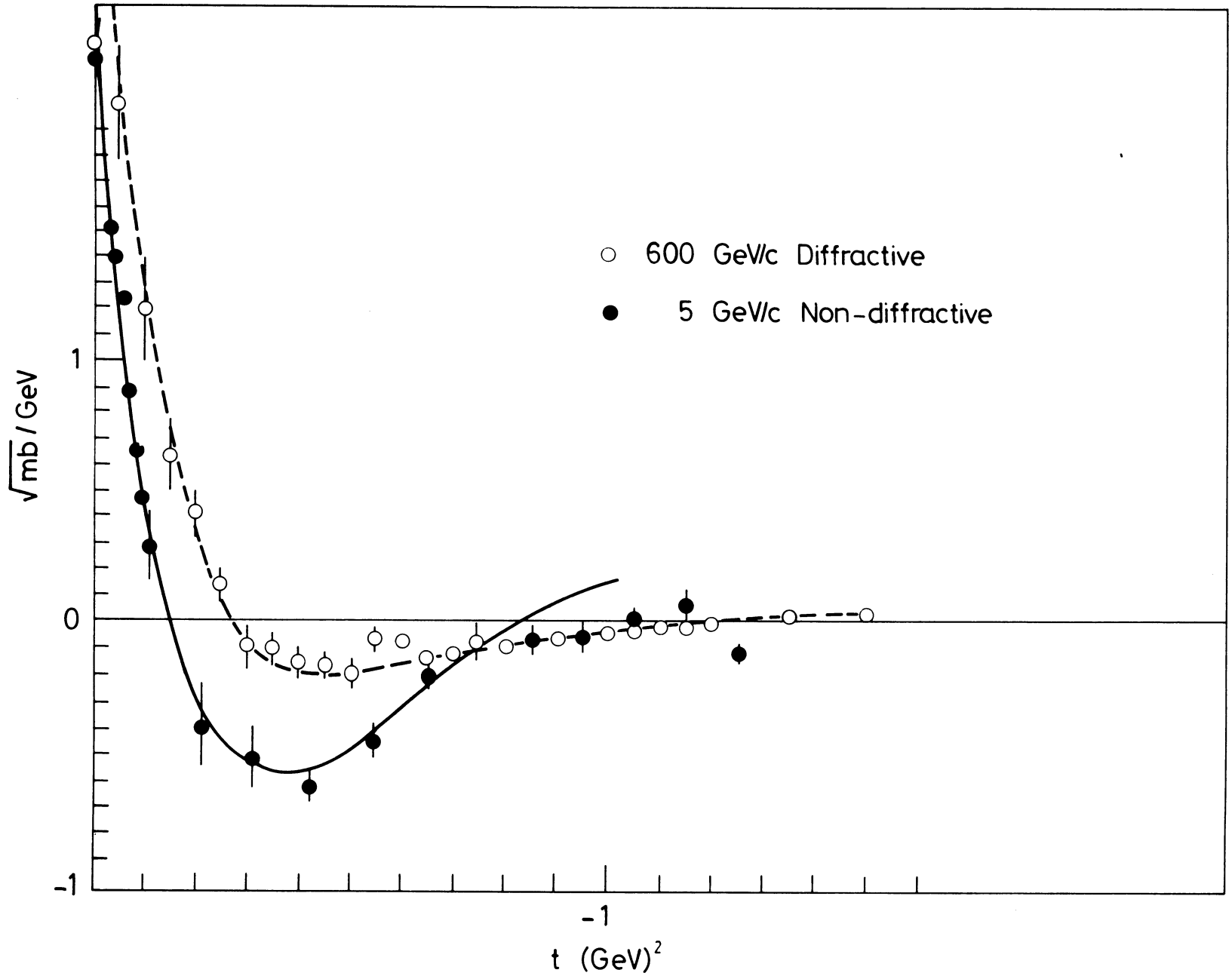
600 GeV/c Diffractive
5 GeV/c Non-diffractive
√mb / GeV
1
0
-1
-1
t (GeV)²

Fig. 4

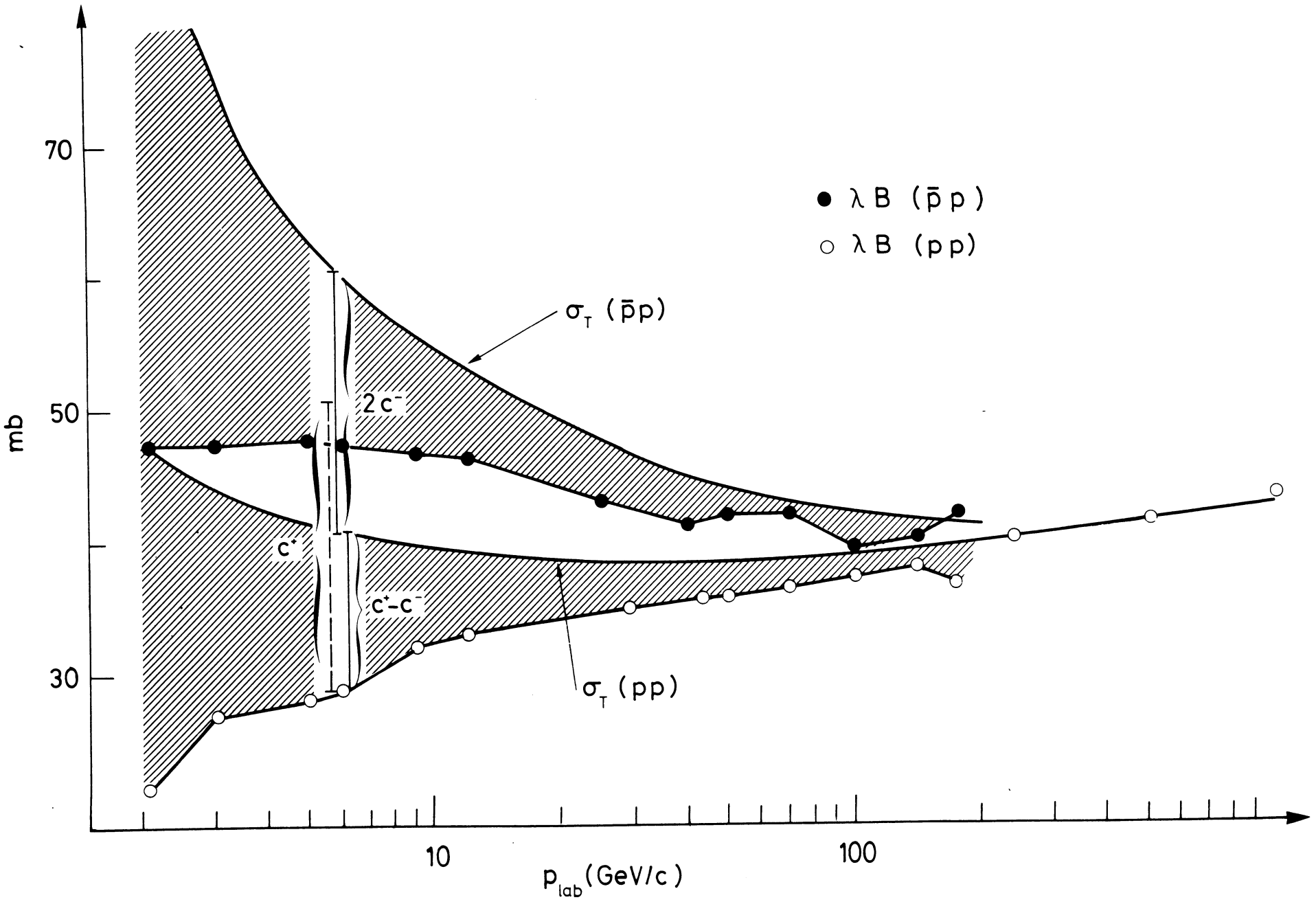

Fig. 5

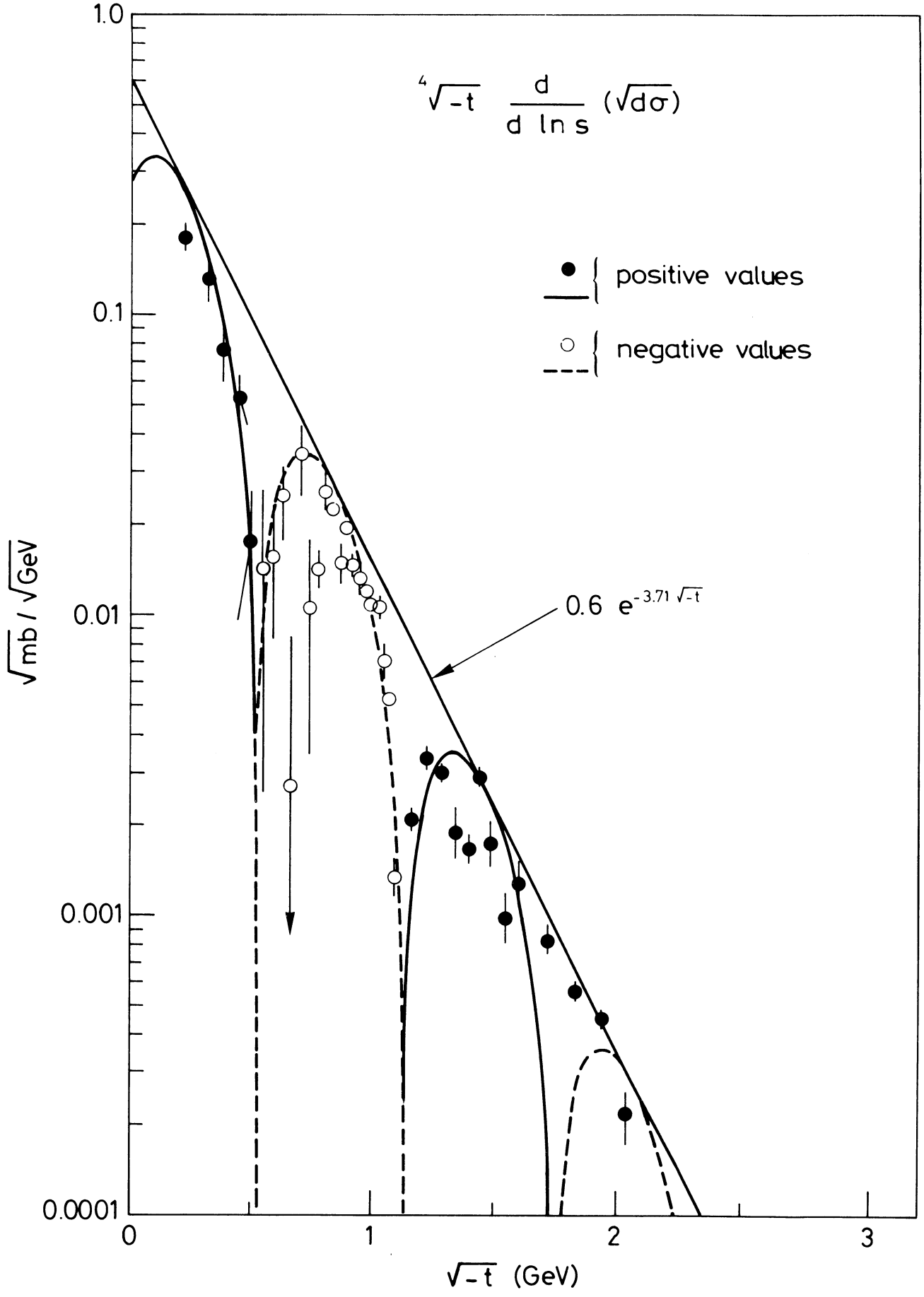
1.0
0.1
0.01
0.001
0.0001
0
1
2
3
$\sqrt{mb}$ / $\sqrt{GeV}$
$\sqrt{-t}$ (GeV)
$\sqrt[4]{-t}\ \frac{d}{d \ln s}(\sqrt{d\sigma})$
positive values
negative values
$0.6\ e^{-3.71\sqrt{-t}}$

Fig. 6

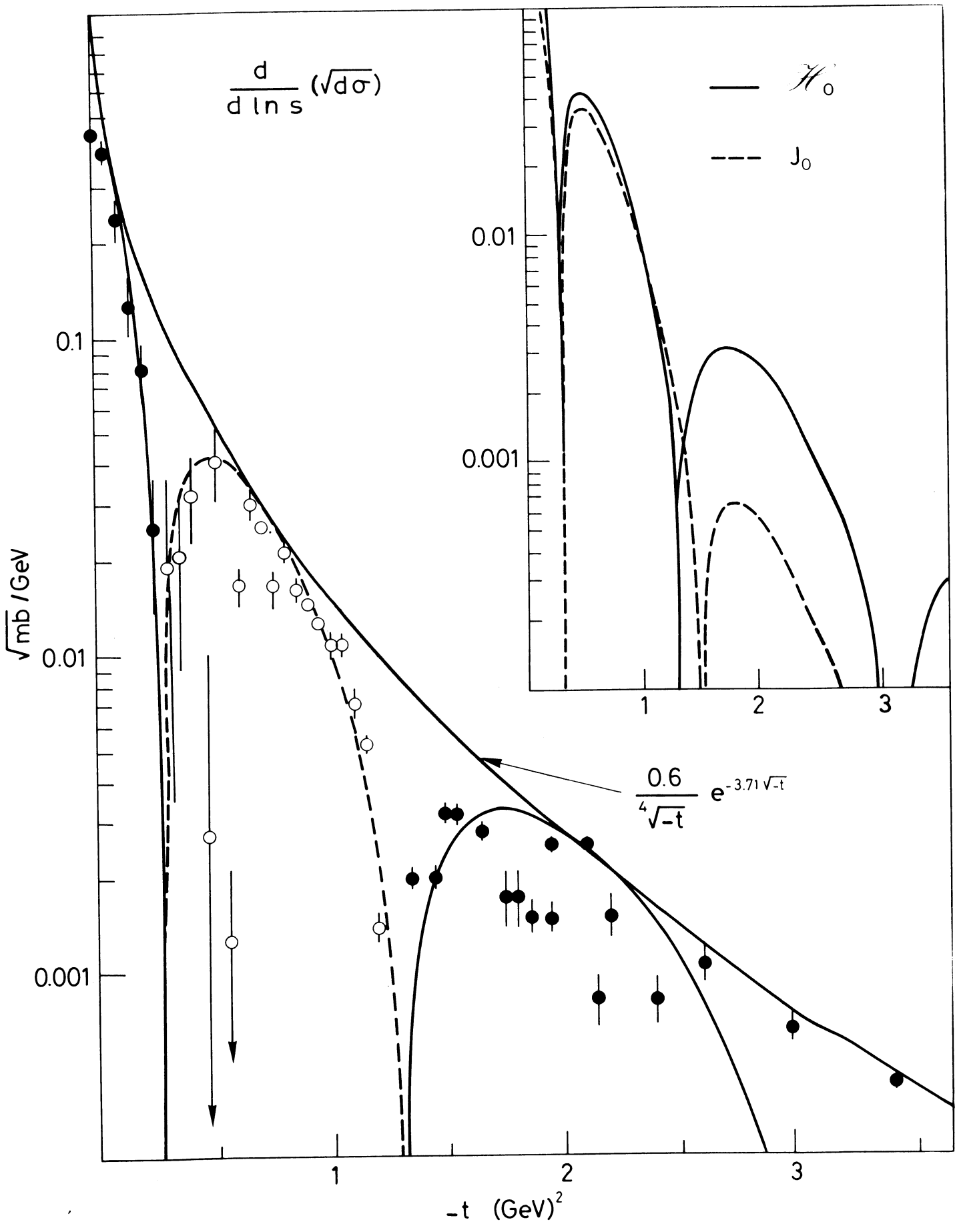
$\frac{d}{d \ln s}(\sqrt{d\sigma})$
$\mathcal{H}_0$
J_0
0.01
0.001
0.1
0.01
0.001
$\sqrt{mb}$ /GeV
$\frac{0.6}{\sqrt[4]{-t}}\, e^{-3.71\sqrt{-t}}$
1
2
3
1
2
3
$-t$ (GeV)^2

Fig. 7

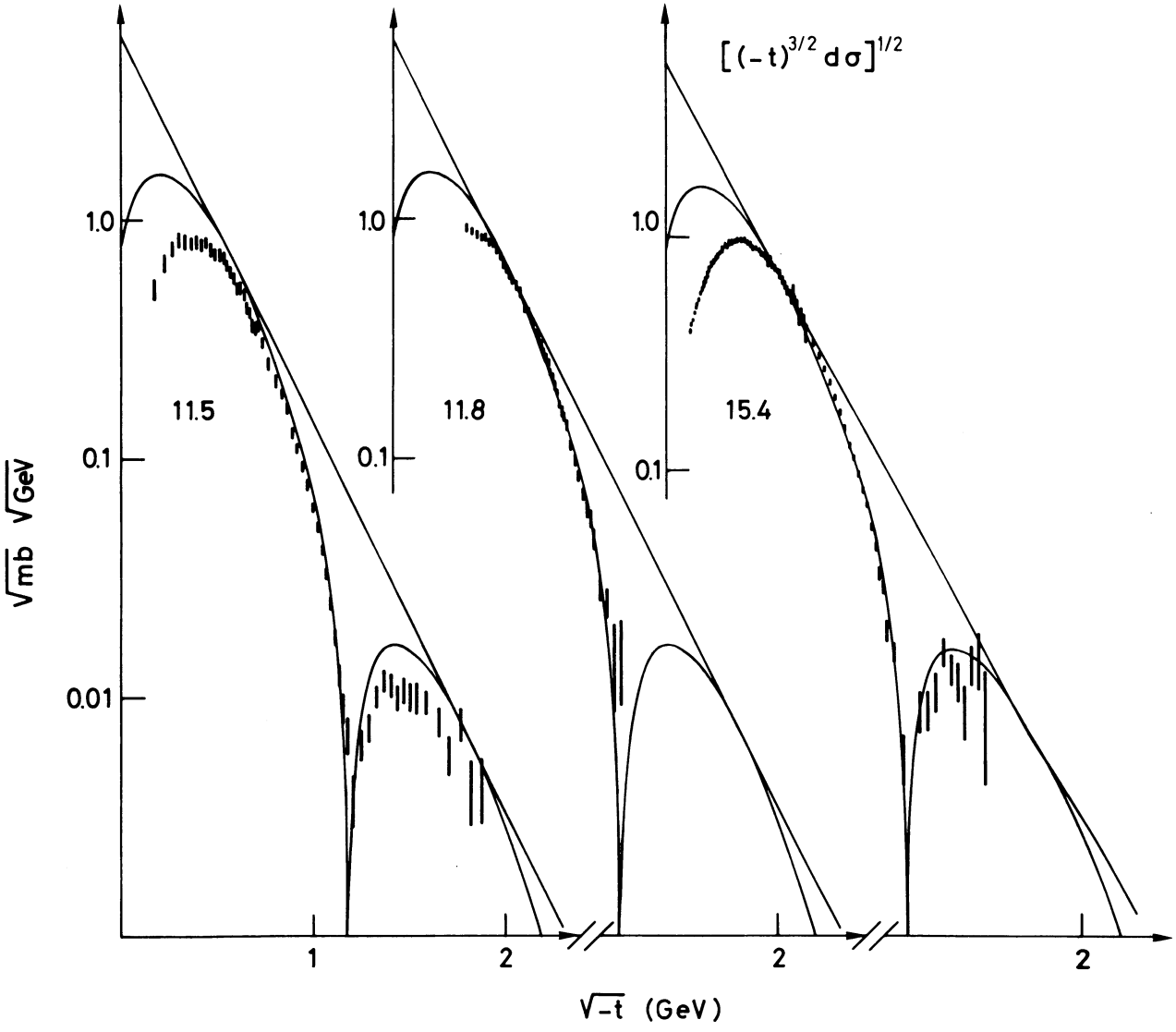
$[(-t)^{3/2}\, d\sigma]^{1/2}$
1.0
0.1
0.01
11.5
11.8
15.4
$\sqrt{mb}\ \sqrt{GeV}$
1
2
2
2
$\sqrt{-t}$ (GeV)

Fig. 8a

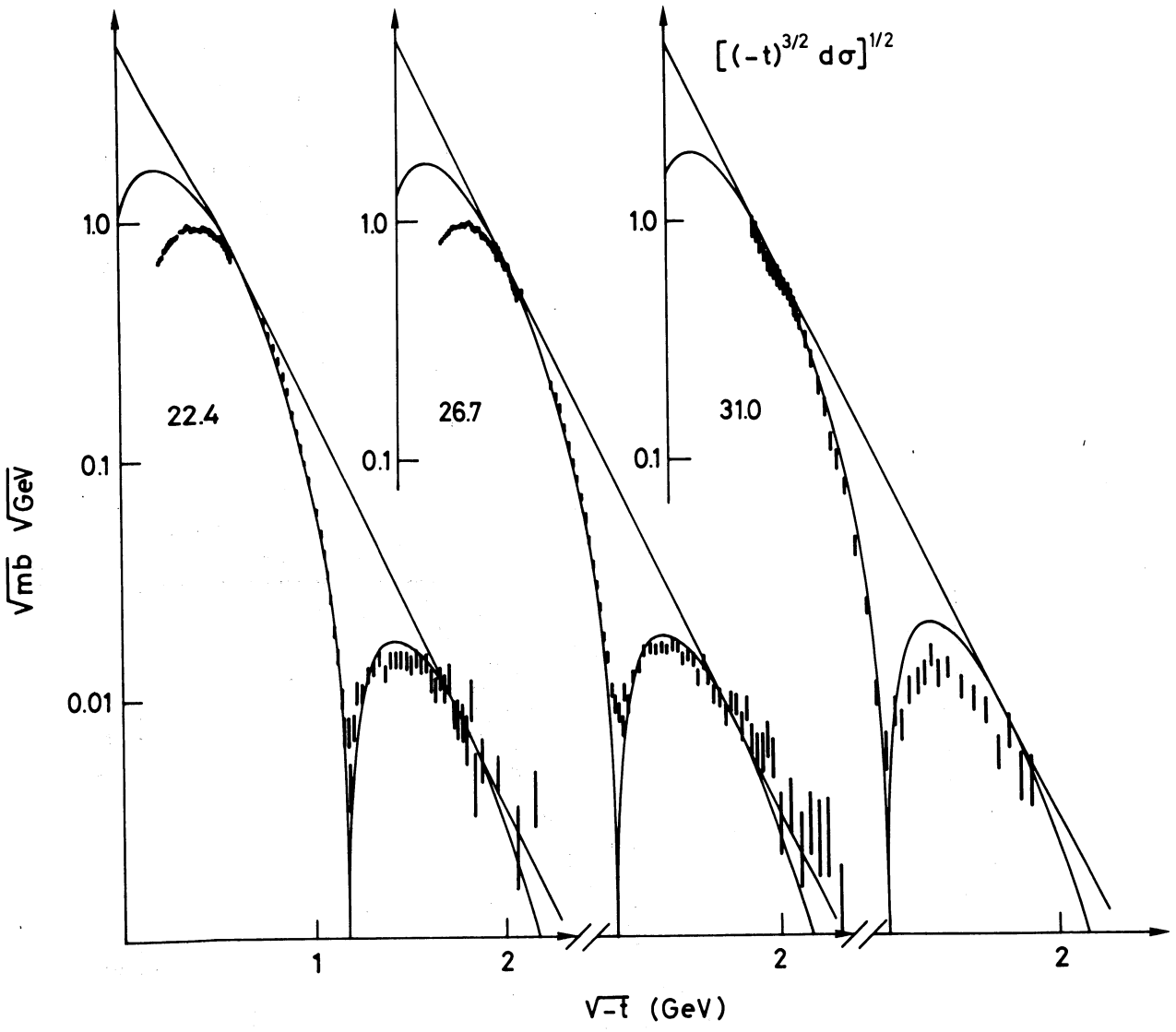
$[(-t)^{3/2}\, d\sigma]^{1/2}$
1.0
0.1
0.01
22.4
26.7
31.0
$\sqrt{mb}\ \sqrt{GeV}$
1
2
2
2
$\sqrt{-t}$ (GeV)

Fig. 8b

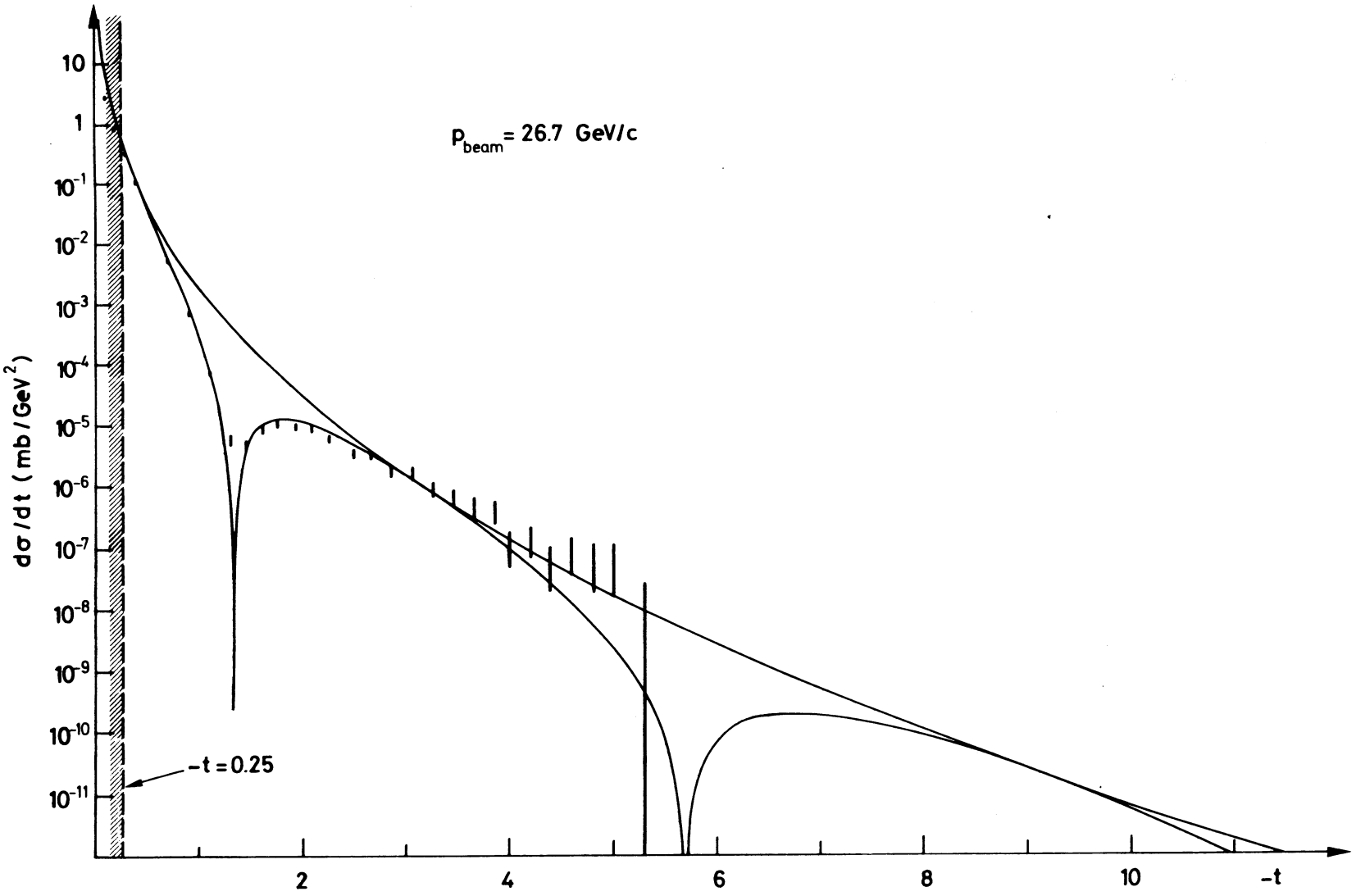
p_{beam} = 26.7 GeV/c
$d\sigma/dt$ (mb/GeV^2)
10
1
10^{-1}
10^{-2}
10^{-3}
10^{-4}
10^{-5}
10^{-6}
10^{-7}
10^{-8}
10^{-9}
10^{-10}
10^{-11}
-t = 0.25
2
4
6
8
10
-t

Fig. 9